



2013

13th Oxford Summer School on Neutron Scattering

Answer Book

A) Coherent and Incoherent Scattering	1
B) Time-of-flight Powder Diffraction	4
C) Single Crystal Diffraction	8
E) Incoherent Inelastic Scattering	14
F) Coherent Inelastic Scattering	16
D) Magnetic Scattering	19
G) Disordered Materials Scattering	23
H) Polarized Neutrons	29
I) High Resolution Spectroscopy	35

The school is supported by:



Science & Technology Facilities Council



<http://www.oxfordneutronschool.org>

2nd – 13th September 2013

A. Coherent and Incoherent Scattering

A1

(1) Hydrogen. b_{coh} is derived by averaging the scattering length over the states with parallel and antiparallel neutron–nucleus spin states, Eq. (B2),

$$b_{\text{coh}} = \bar{b} = w^+ b^+ + w^- b^-$$

The weights are given by Eq. (A1): $w^+ = (I+1)/(2I+1)$ and $w^- = I/(2I+1)$. Setting $I = \frac{1}{2}$ we have $w^+ = \frac{3}{4}$ and $w^- = \frac{1}{4}$. From Table A1,

$$\begin{aligned} b_{\text{coh}} &= \frac{3}{4}(10.85) + \frac{1}{4}(-47.5) \text{ fm} \\ &= -3.74 \text{ fm} \end{aligned}$$

The coherent scattering cross section is given by Eq. (A3),

$$\begin{aligned} \sigma_{\text{coh}} &= 4\pi b_{\text{coh}}^2 \\ &= 1.75 \text{ b} \quad (1 \text{ b} = 10^{-28} \text{ m}^2) \end{aligned}$$

The total cross section is obtained by summing the weighted values of the spin states of the combined nucleus-neutron system, Eq. (A4):

$$\begin{aligned} \sigma_{\text{tot}} &= 4\pi\{w^+(b^+)^2 + w^-(b^-)^2\} \\ &= 81.7 \text{ b} \end{aligned}$$

Finally, the incoherent scattering cross section is the difference between σ_{tot} and σ_{coh} ,

$$\begin{aligned} \sigma_{\text{inc}} &= \sigma_{\text{tot}} - \sigma_{\text{coh}} \\ &= 79.9 \text{ b} \end{aligned}$$

(1) Deuterium. For $I = 1$ we have from Eq. (A1), $w^+ = \frac{2}{3}$ and $w^- = \frac{1}{3}$. From the data in Table A1, and the formulae above,

$$b_{\text{coh}} = 6.67 \text{ fm}$$

$$\underline{\sigma_{\text{coh}} = 5.6 \text{ b}}$$

$$\underline{\sigma_{\text{tot}} = 7.6 \text{ b}}$$

$$\underline{\sigma_{\text{inc}} = 2.0 \text{ b}}$$

A2

In this example the incoherent scattering is mainly isotopic in origin, but there is a small contribution from the spin.

The coherent scattering length is the weighted average of the scattering lengths of the different isotopes, Eq. (A2):

$$b_{\text{coh}} = \bar{b} = \sum_r c_r (w_r^+ b_r^+ + w_r^- b_r^-)$$

Using Table A1a below we have:

$$\underline{b_{\text{coh}} = 10.34 \text{ fm}}$$

The coherent scattering cross section is given by Eq. (A3),

$$\begin{aligned} \sigma_{\text{coh}} &= 4\pi b_{\text{coh}}^2 = 4\pi \bar{b}^2 \\ &= \underline{13.43 \text{ b}} \end{aligned}$$

The total scattering cross section is given by Eq. (A4),

$$\sigma_{\text{tot}} = 4\pi \sum_r c_r \{w_r^+(b_r^+)^2 + w_r^-(b_r^-)^2\}$$

where,

$$w_r^+ = \frac{I_r+1}{2I_r+1} \text{ and } w_r^- = \frac{I_r}{2I_r+1}$$

Hence,

$$\underline{\sigma_{\text{tot}} = 18.50 \text{ b}}$$

Finally, from Eq. (A5), $\sigma_{\text{inc}} = \sigma_{\text{tot}} - \sigma_{\text{coh}}$, we find that

$$\underline{\sigma_{\text{inc}} = 5.09 \text{ b}}$$

Table A1a

isotope, r	spin I_r	$w_r^+ b_r^+$ (fm)	$w_r^- b_r^-$ (fm)	$w_r^+ (b_r^+)^2$ (b)	$w_r^- (b_r^-)^2$ (b)
58	0	9.883	0	1.416	0
60	0	0.73	0	0.020	0
61	3/2	2.88	4.73	0.132	0.595
62	0	0.31	0	0.027	0
64	0	0.00	0	0.000	0

B. Time-of-Flight Powder Diffraction

B1.

(a) The expression

$$t = \left(\frac{m_n}{h} \right) \lambda L$$

follows from the relations

$$L = vt$$

$$\lambda = \frac{h}{m_n v}$$

Where v is the neutron velocity.

From the values of h and m_n on page 41 we get

$$t (\mu\text{secs}) = 252.8 \times \lambda (\text{\AA}) \times L (\text{m}) \quad (\text{B1a})$$

(b) In Bragg scattering from lattice planes HKL of spacing d_{HKL} the wavelength of the scattered radiation is given by

$$\lambda = 2d_{HKL} \sin \theta \quad (\text{B2a}) \quad \text{ssdfsdfsdfsdfsdfsdfsdfs}$$

where 2θ is the scattering angle. Putting $L = 100$ m into eqn. (B1a) and $\theta = 85^\circ$ into eqn. (B2a) gives

$$t (\mu\text{secs}) = 5.035 \times 10^4 d_{HKL} (\text{\AA}) \quad (\text{B3a})$$

Perovskite has a primitive cubic lattice, so that the first three Bragg reflections (corresponding to the longest times-of-flight) are 100 , 110 and 111 . The d-spacing is related to the lattice constant a_0 by

$$d_{HKL} = a_0 (H^2 + K^2 + L^2)^{-1/2} \quad (\text{B4a})$$

Therefore; $d_{100} = 3.84$ Å, $d_{110} = 2.72$ Å and $d_{111} = 2.22$ Å.

Substituting into eqn. (B3a) we find that

$$t_{100} = 194 \text{ ms}, t_{110} = 137 \text{ ms} \text{ and } t_{111} = 112 \text{ ms.}$$

(c) Combining eqns. (B3a) and (B4a) gives:

$$t \propto (H^2 + K^2 + L^2)^{-1/2} \quad (\text{B5a})$$

B2.

(a) The *Structure Factor* F_{HKL} , or the amplitude of the scattering into the HKL Bragg reflection by the atoms in one unit cell, is given by:

$$F_{(HKL)} = \sum_n b_n \exp [i2\pi(Hx_n + Ky_n + Lz_n)] \quad (\text{B6a})$$

Here b_n is the scattering length of the n^{th} nucleus in the cell, $x_n y_n z_n$ are its fractional coordinates. The sum is taken over all atoms in the unit cell.

In the diamond structure of silicon there is a basis of two silicon atoms at

$0,0,0$ and $\frac{1}{4},\frac{1}{4},\frac{1}{4}$

and this basis is distributed at each of the face-centred-cubic lattice points:

$0,0,0; \quad \frac{1}{2},\frac{1}{2},0; \quad \frac{1}{2},0,\frac{1}{2}; \quad 0,\frac{1}{2},\frac{1}{2}$

There are therefore 8 atoms in the unit cell, with fractional coordinates

$(0,0,0; \quad \frac{1}{2},\frac{1}{2},0; \quad \frac{1}{2},0,\frac{1}{2}; \quad 0,\frac{1}{2},\frac{1}{2})$ for $n = 1$ to 4

and

$\frac{1}{4},\frac{1}{4},\frac{1}{4} + (0,0,0; \quad \frac{1}{2},\frac{1}{2},0; \quad \frac{1}{2},0,\frac{1}{2}; \quad 0,\frac{1}{2},\frac{1}{2})$ for $n = 5$ to 8

Inserting these coordinates into eqn. (B6a) gives:

$$\begin{aligned} F_{(HKL)} = b_{Si} & \left\{ 1 + e^{i\pi(H+K)} + e^{i\pi(H+L)} + e^{i\pi(K+L)} \right. \\ & + e^{i\frac{\pi}{2}(H+K+L)} + e^{i\frac{\pi}{2}(3H+3K+L)} \\ & \left. + e^{i\frac{\pi}{2}(3H+K+3L)} + e^{i\frac{\pi}{2}(H+3K+3L)} \right\} \end{aligned}$$

This then can be written,

$$\begin{aligned} F_{(HKL)} = b_{Si} & \left\{ 1 + e^{i\pi(H+K)} + e^{i\pi(H+L)} + e^{i\pi(K+L)} \right\} \\ & \times \left\{ 1 + e^{i\frac{\pi}{2}(H+K+L)} \right\} \quad (\text{B7a}) \end{aligned}$$

If H , K and L are mixed odd or even numbers, then the term in the first {} bracket is zero. (2 out of the 3 exponential terms is -1, the third is +1)

(b) A further restriction on the indices of the Bragg reflections is imposed by the second bracket {} in eqn. (B7a). If $\frac{1}{2}(H+K+L)$ is even, this bracket is equal to 2; if $\frac{1}{2}(H+K+L)$ is odd, the bracket is zero.

(c)

(i) The possible values of HKL for the f.c.c. lattice are shown in Table C.1a.

Table B1a

Sums of three squared integers/ Miller indices.

$H^2+K^2+L^2 / HKL$	$H^2+K^2+L^2 / HKL$	$H^2+K^2+L^2 / HKL$	$H^2+K^2+L^2 / HKL$
3* 111	12* 222	21	32* 440
4* 200	13	22	33
5	14	24* 422	34
6	16* 400	25	35* 531
8* 220	17	26	36* 600/442
9	18	27* 511/333	37
10	19* 331	29	38
11* 311	20* 420	30	40* 620

(ii) The forbidden reflections are: 200, 222, 420, 600/442

(iii) The overlapping reflection is: 511/333

(d) Putting $L = 96.8$ m into eqn. (B1a) and $\theta = 45.4^\circ$ into eqn. (B2a) gives

$$t \text{ (ms)} = 34.848 d_{HKL} \text{ (\AA)} \quad (\text{B8a})$$

111 is the Bragg peak with the longest flight time. The next peak is 220 (200 is forbidden). Thus 220 is peak no 2 in Figure B1. Using the information in section (c) the remaining peaks are readily indexed (see Table B1a below).

Table B2a

	time of flight (ms)	<i>d</i> -spacing	<i>HKL</i>	$H^2+K^2+L^2$	$a_0 = d_{HKL} \times \sqrt{H^2 + K^2 + L^2}$
1	109.232	3.1399	111	3	5.42916
2	66.912	1.9234	220	8	5.43089
3	57.066	1.6404	311	11	5.43120
4	47.320	1.3602	400	16	5.43159
5	43.424	1.2482	331	19	5.43161
6	38.636	1.1106	422	24	5.43150
7	36.426	1.0471	511/333	27	5.43145
8	33.457	0.9617	440	32	5.43105
9	31.991	0.9196	531	35	5.43105
10	29.923	0.8605	620	40	5.43072

Taking the mean of the lattice constant calculated from the peaks – excluding the first peak – we get for the lattice constant of Si.

$$a_0 = 5.4312 \text{ \AA}$$

The calculation from the first peak is slightly out due to a higher order term in the time-of-flight to *d*-spacing conversion. This comes about due to the fact that the total flight path of the neutron is related to the wavelength. In general, short wavelength neutrons will penetrate further into the sample than long wavelength neutrons, and so the total flight path therefore becomes a function of both 2θ and λ .

Observed times-of-flight of reflections may be noticeably different from those expected from the expression C8a, especially at longer *d*-spacings (which are measured with neutrons of longer wavelength, where absorption is greater). Empirically, it is found that a quadratic dependence provides a good description of the shifts in the reflection positions.

In GSAS for example, each diffraction bank is characterised by three constants. DIFC (which is the constant $252.82 \times L \sin \theta$ that we calculated above), DIFA – proportional to d^2 and ZERO, which accounts for any offset in the measured timing of the data acquisition system. Altogether this gives

$$t (\mu\text{secs}) = 252.8 \times \text{DIFC } d_{HKL} (\text{\AA}) + \text{DIFA } d_{HKL}^2 (\text{\AA}^2) + \text{ZERO} \quad (\text{C9a})$$

These diffractometer constants are fixed by the instrument parameters, and should not be refined.

C. Single-Crystal Diffraction

C1.

(i) From the relation $\lambda = h/(m_n v)$ we get

$$\lambda (\text{\AA}) = 3.956 / v (\text{km s}^{-1}).$$

Putting $v = 2.20 \text{ km s}^{-1}$ gives $\lambda = 1.798 \text{ \AA}$.

(ii) Similarly from $E = \frac{1}{2}m_n v^2$ we obtain $E = 25.30 \text{ meV}$.

(iii) The X-ray energy is given by:

$$E_{X-Ray} = h\nu = \frac{hc}{\lambda}$$

with ν the frequency of the X-rays and c the velocity of light.

Putting $c = 3 \times 10^8 \text{ ms}^{-1}$ gives

$$E = 6.88 \text{ keV}$$

(iv) The velocity of a neutron with this energy is

$$v = \left(\frac{2E}{m_n} \right)^{\frac{1}{2}}$$

therefore, $v = 1148 \text{ km s}^{-1}$

We see then that thermal neutrons have both wavelengths suitable for studying atomic structures in the 1-100 Å range and energies suitable for studying excitations (such as phonons or magnons) in the meV range. (Fast neutrons have too short a wavelength and are too energetic for either purpose.)

C2

(i). The wavelength of the reflected beam is

$$\lambda = 2d_{111} \sin\theta$$

where $d_{111} = a_0 / \sqrt{3}$. Thus $\sin\theta = 1.8 / 5.7$ and the scattering angle is

$$2\theta = 36.7^\circ$$

(ii). The wavelength spread is derived by differentiating Bragg's equation:

$$\frac{\Delta\lambda}{\lambda} = -\cot\theta \cdot \Delta\theta$$

Putting $\Delta\theta = 0.2^\circ$ gives $\frac{\Delta\lambda}{\lambda} = 0.0105$, so that for $\lambda = 1.8 \text{ \AA}$ we get

$$\Delta\lambda = \pm 0.019 \text{ \AA}$$

Note that this spread of wavelengths is much larger than the natural width of characteristic X-ray lines, and so Bragg peaks obtained with neutrons will not be as sharp as X-ray peaks.

C3

Figure C1a shows the reciprocal lattice in the $a^* b^*$ plane, together with the Ewald circles passing through the reflections (630) and (360).

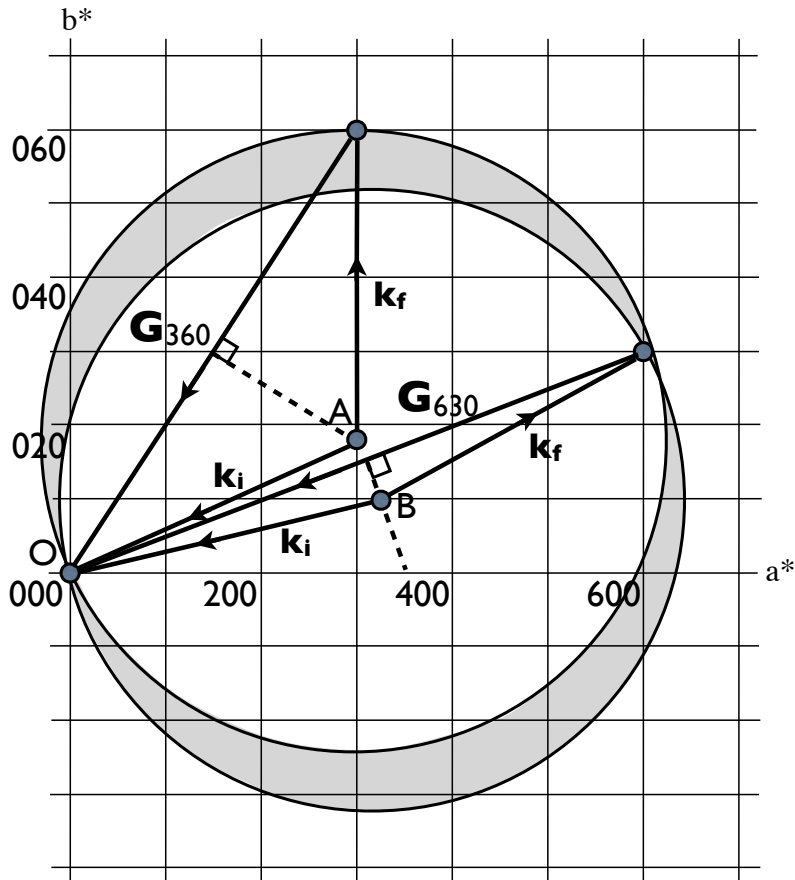


Figure C1a. The Ewald circles for the (630) and (360) reflections. A is the centre of the circle for (360) and B is the centre of the circle for (630).

We can consider the crystal to be stationary and the incident beam to turn between the directions $\mathbf{AO} \rightarrow$ and $\mathbf{BO} \rightarrow$ in the Figure. During this rotation the area swept out in reciprocal space is the shaded region. The number of reciprocal lattice points in this region, i.e. the number of Bragg reflections, is approximately 16.

C4

Figure C2a shows the Ewald circles drawn for the two extreme wavelengths. The observable reflections are those lying in the shaded area lying between the two circles. For a primitive unit cell there are

no systematically absent reflections, and so the number of possible reflections is about 40.

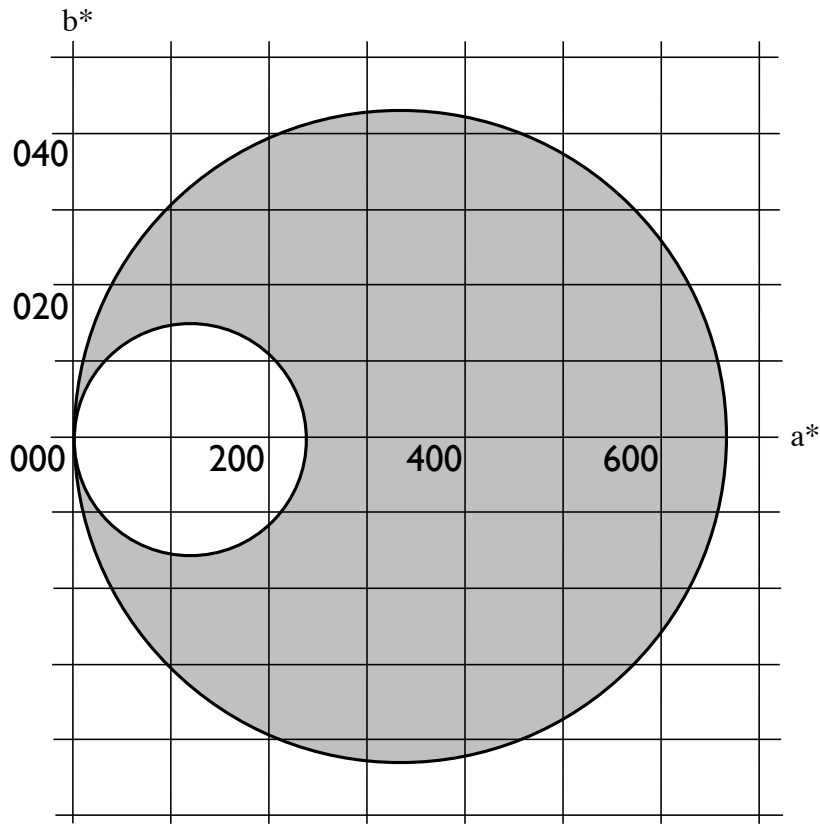


Figure C2a. The Ewald construction showing the reflection circles for the minimum wavelength (maximum radius) and the maximum wavelength (minimum radius).

C5

- (i) The intensity of the $(00L)$ reflection is proportional to the square of the structure factor;

$$F_{(HKL)} = \sum_n b_n \exp [i2\pi(Hx_n + Ky_n + Lz_n)]$$

Where the sum is over the atoms in the unit cell of the crystal.
Therefore the structure factor for the $(00L)$ reflection is;

$$\begin{aligned} F_{(00L)} &= b_{Ba} \exp [0] + b_{Ti} \exp [i\pi L] + b_O \exp [0] + 2b_O \exp [i\pi L] \\ &= b_{Ba} + (-1)^L b_{Ti} + [1 + 2(-1)^L] b_O \end{aligned}$$

$I_{(00L)}$ is therefore proportional to the square of this expression.

(ii) For the (005) reflection, we can substitute the scattering lengths to find

$$F_{(005)} = 5.25 + 3.30 - 5.81 = 2.74$$

and therefore

$$I_{(005)} \propto |F_{(005)}|^2 = 7.51$$

For the distorted case we have the structure factor;

$$\begin{aligned} F_{(005)}^\delta &= \sum_n b_n \exp[i2\pi L(z_n + \delta_n)] \\ &= \sum_n b_n \exp[i2\pi Lz_n] \exp[i2\pi L\delta_n] \end{aligned}$$

where $\delta_n = 0$ for the Ba atoms, $+\delta$ for the Ti atoms, $-\delta$ for the O atoms, and $L = 5$. Writing this out in full as before, we have

$$F_{(005)}^\delta = b_{Ba} - b_{Ti} \exp(i10\pi\delta) - b_O \exp(-i10\pi\delta)$$

Assuming small displacements, we can expand the exponential terms to first order, giving

$$\begin{aligned} F_{(005)}^\delta &= b_{Ba} - b_{Ti}(1 + i10\pi\delta) - b_O(1 - i10\pi\delta) \\ &= 2.74 + i286\delta \end{aligned}$$

and therefore

$$\begin{aligned} I_{(005)}^\delta \propto |F_{(005)}^\delta|^2 &= (2.74 + i286\delta)(2.74 - i286\delta) \\ &= 7.51 + 81796\delta^2 \end{aligned}$$

Since the Bragg peak intensity increases by 74% due to the distortion, we can write

$$\begin{aligned} \frac{I_{(005)}^\delta}{I_{(005)}} &= \frac{7.51 + 81796\delta^2}{7.51} = 1.74 \\ &\Rightarrow 10891\delta^2 = 0.74 \\ &\Rightarrow \delta = 0.0083 \end{aligned}$$

[remember that this is the distortion expressed as a fraction of the lattice constant]

(iii) For the X-ray case, the structure factors are proportional to

$$\begin{aligned} F_{(005)} &= 56 - 22 - 8 = 26 \\ F_{(005)}^\delta &= 56 - 22(1 + i10\pi\delta) - 8(1 - i10\pi\delta) \\ &= 26 + i440\delta \end{aligned}$$

so now the ratio of the intensities becomes

$$\begin{aligned} \frac{I_{(005)}^\delta}{I_{(005)}} &= \frac{676 + 193600\delta^2}{676} \\ &= 1 + 286 \times (0.0083)^2 \\ &= 1.019 \end{aligned}$$

So the increase in intensity of the (005) reflection is only 1.9% compared to the undistorted structure. This is due to a number of factors, including the greater sensitivity of neutrons to oxygen atoms, the negative scattering amplitude of the Ti, and the fact that the X-ray structure factor is dominated by the Ba atom, which does not move under the distortion.

D. Incoherent Inelastic Scattering (with a Pulsed Neutron Spectrometer)

D1.

- (i) The elastic peak in Figure D2 occurs at the t.o.f.:

$$t \simeq 64.1 \text{ ms}$$

The total flight path is $36.54 \text{ m} + 1.47 \text{ m} = 38.01 \text{ m}$, and so the neutron velocity is

$$v_n = 0.593 \text{ km s}^{-1}$$

and the energy selected by the crystal analyser is

$$E_n = \frac{1}{2}m_nv_n^2 = 1.85 \text{ meV}$$

- (ii) The Bragg angle θ_A of the analyser is given by

$$\theta_A = \sin^{-1}(\lambda/2d_{002})$$

where $\lambda = h/m_nv_n = 6.67 \text{ \AA}$. Thus $\theta_A \simeq 85^\circ$

- (iii) The advantage of using a high take-off angle of $2\theta = 170^\circ$ is that the wavelength band reflected by the analyser is then relatively small.

D2.

For neutron-energy gain the flight-time is greater than it is for elastic scattering, whereas for neutron-energy loss the flight-time is less than for elastic scattering. So the inelastic peaks in Figure D2 are at $t \simeq 65.7 \text{ ms}$ for energy gain and at $t \simeq 62.7 \text{ ms}$ for energy loss.

The sample-analyser-detector distance is 1.47 m and the total flight-path is 38.01 m. The elastically scattered neutrons cover the total flight path in 64.1 ms, and so they cover the sample-analyser-detector distance in $64.1 \times (1.47/38.01) = 2.48 \text{ ms}$. The moderator-to-sample distance of 36.54 m is covered by the energy-gain neutrons in the time

$$65.7 - 2.48 \text{ ms} = 63.2 \text{ ms.}$$

Hence the initial energy of these neutrons is

$$E_{gain}^i = \frac{1}{2} m_n v_n^2 = \frac{1}{2} m_n (36.54/0.0632)^2$$

giving, $E_{gain}^i = 1.76 \text{ meV}$

A similar calculation for the energy-loss neutrons gives

$$E_{loss}^i = 1.94 \text{ meV}$$

Therefore, the energy transfer to/from the sample is half the difference between the peak energies,

$$\Delta E = \pm 0.09 \text{ meV}$$

D3

(i) The intensity is influenced by the Bose factor $n(E)$ which is proportional to the number of phonons which exist at a given energy $E = \hbar\omega$ and temperature T (since phonons are bosons).

$$n(E) = \frac{1}{\exp\left(\frac{\hbar\omega}{k_B T}\right) - 1}$$

Due to the “Law of Detailed Balance” the intensity on the neutron energy loss side (often called the “Stokes” side by light scatterers) is proportional to $[1 + n(E)]$

For neutron energy gain (called the “anti-Stokes” side) the intensity is proportional to $n(E)$. At low temperatures $n(E)$ tends to zero and only scattering with neutron energy loss is possible. There is always a greater possibility, at any temperature, that neutrons will be scattered with energy loss.

E. Coherent Inelastic Scattering (with a Three-Axis Spectrometer)

E1.

The allowed points have HKL indices, which are all odd or all even. See Figure E1a.

E2.

The relation between neutron energy E and neutron wave number k is

$$E \text{ (meV)} = 2.072 [k \text{ (\AA}^{-1})]^2$$

Putting $E_i^{\min} = 3 \text{ meV}$ and $E_i^{\max} = 14 \text{ meV}$ gives

$$k_i^{\min} = 1.203 \text{ \AA}^{-1} \text{ and } k_i^{\max} = 2.600 \text{ \AA}^{-1}$$

Since $k = 2\pi / \lambda$, k_i^{\min} corresponds to the maximum wavelength $\lambda_i^{\max} = 5.22 \text{ \AA}$, and k_i^{\max} to the minimum wavelength $\lambda_i^{\min} = 2.42 \text{ \AA}$

E3

(i) We have $Q_{220} = 2\pi / d_{220} = \sqrt{8}(2\pi / a_0)$ so that $Q_{220} = 3.20 \text{ \AA}$.

Figure F1a shows the vectors \mathbf{k}_i , \mathbf{k}_f and \mathbf{Q} for the 220 reflection.

(ii) Setting $\mathbf{k}_i = \mathbf{k}_f$ in the scattering triangle equation;

$$\mathbf{Q} = \mathbf{k}_i^2 + \mathbf{k}_f^2 - 2\mathbf{k}_i\mathbf{k}_f \cos\phi$$

we get

$$\phi = 2 \sin^{-1} (Q/2k_i)$$

and so

$$\phi = 75.9^\circ$$

(iii) In the case of elastic scattering the scattering angle ϕ is twice the Bragg angle θ_B

E4.

See Figure E1a.

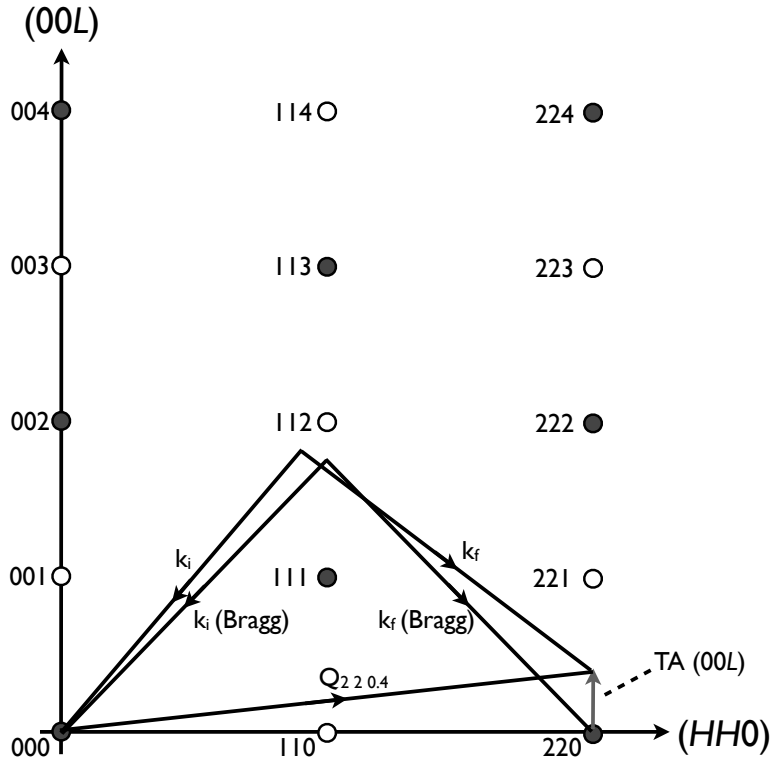


Figure E1a. Reciprocal lattice construction for 220 Bragg scattering and for inelastic scattering by the transverse acoustic [00L] phonon.

E5.

The vector $\mathbf{Q}_{220.4}$ (Figure F1a) has a magnitude of

$$Q_{220.4} = (2\pi / a_0) \times \sqrt{(4 + 4 + 0.16)} = 3.228 \text{ \AA}^{-1}$$

We have $E_i^{max} = 14 \text{ meV}$ and $\Delta E = 3 \text{ meV}$. Hence for neutron energy loss $E_f = 3 \text{ meV}$ and for neutron energy gain $E_f = 3 \text{ meV}$. Using eqn. (E4) we get $k_f = 2.304 \text{ \AA}^{-1}$ for energy loss and $k_f = 2.864 \text{ \AA}^{-1}$ for energy gain. From eqn. (E2) we then have $\phi = 82.1^\circ$ (energy loss) and $\phi = 72.2^\circ$ (energy gain).

F6.

The resolution is best for small k_f , i.e. for energy loss. In Figure E1a the vectors \mathbf{k}_i and \mathbf{k}_f are drawn for this configuration.

E7.

(i) At 300K: $n(E) = 8.3$ for energy gain and $n(E) + 1 = 9.3$ for energy loss.

At 0K: $n(E)=0$ for energy gain and $n(E) + 1 = 1$ for energy loss.

(ii) Thus it doesn't make much difference at 300K whether one works in energy gain or in energy loss, but at low temperatures one must work in energy loss.

E8.

No. Not with this value of the incident wavelength.

We have

$$Q_{440} = 2Q_{220} = 6.46 \text{ \AA}^{-1}$$

$k_i + k_f = 4.904 \text{ \AA}^{-1}$ in energy loss, and $k_i + k_f = 5.464 \text{ \AA}^{-1}$ in energy gain. Hence $k_i + k_f < Q$ and it is impossible to close the scattering triangle (Figure E2) in either case.

E9.

Since potassium is cubic, the dispersion relationship shown in Fig. F9 for $\mathbf{q} \parallel$ to (001) also applies to $\mathbf{q} \parallel$ to (100). The LA mode (longitudinal acoustic) will have a higher frequency for a given \mathbf{q} than the TA (transverse acoustic) mode (due to Hooke's Law – transverse modes cause less longitudinal displacement than transverse modes).

$\mathbf{Q} = [2.5 \ 0 \ 0]$ is equivalent to $\mathbf{Q} = [0 \ 0 \ 0.5]$. Therefore, reading from the plot gives the phonon energy for the LA $[0.5 \ 0 \ 0]$ as ~ 1.70 THz, and for the TA $[0.5 \ 0 \ 0]$ as ~ 1.55 THz.

The final energy is fixed at $E_f = 3.5$ THz, so for neutron energy loss

$$\mathbf{E}_i = 3.5 + 1.70 = 5.2 \text{ THz.}$$

F. Magnetic Elastic Scattering

F1.

The equation for a Gaussian is:

$$f(x) = \frac{1}{\sqrt{2\pi\sigma^2}} \exp\left(-\frac{x^2}{2\sigma^2}\right)$$

The Fourier transform of this Gaussian is:

$$F(q) = \exp\left(-\frac{1}{2}q^2\sigma^2\right)$$

The convolution theorem is:

$$\Im(f(x) \otimes g(x)) = F(q) \times G(q)$$

Take two Gaussians, $f(x)$ and $g(x)$, with widths σ_1 and σ_2 . The Fourier transform of the convolution is:

$$\begin{aligned} \Im(f(x) \otimes g(x)) &= \exp\left(-\frac{1}{2}q^2\sigma_f^2\right) \times \exp\left(-\frac{1}{2}q^2\sigma_g^2\right) \\ &= \exp\left(-\frac{1}{2}q^2(\sigma_f^2 + \sigma_g^2)\right) \end{aligned}$$

This may now be inverse Fourier transformed to give:

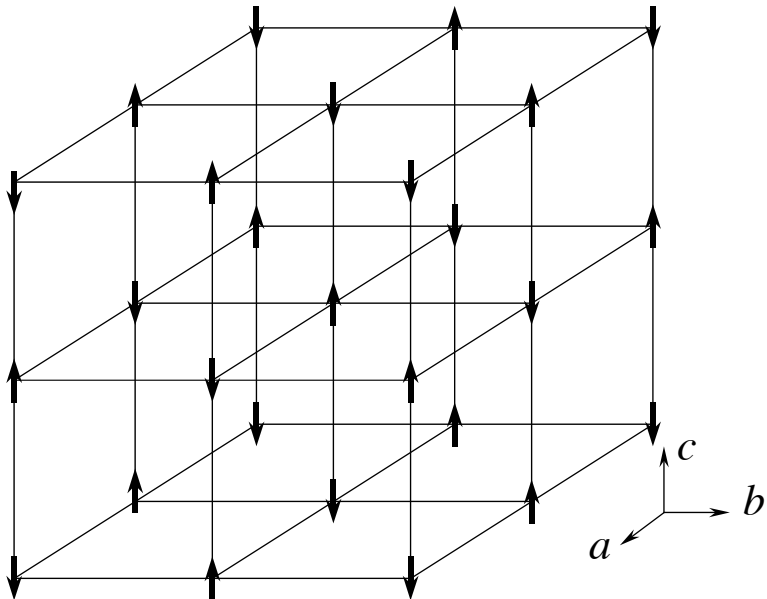
$$\begin{aligned} f(x) \otimes g(x) &= \Im^{-1}(\Im(f(x) \otimes g(x))) \\ &= \frac{1}{\sqrt{2\pi(\sigma_f^2 + \sigma_g^2)}} \exp\left(-\frac{x^2}{2(\sigma_f^2 + \sigma_g^2)}\right) \end{aligned}$$

Hence, the convolution of two Gaussians gives a Gaussian, and its width is given by

$$\sqrt{\sigma_f^2 + \sigma_g^2}$$

F2.1

The moments point along c and each atom is antiferromagnetically coupled to its nearest neighbour, i.e. the magnetic unit cell is twice as large along a , b , and c :

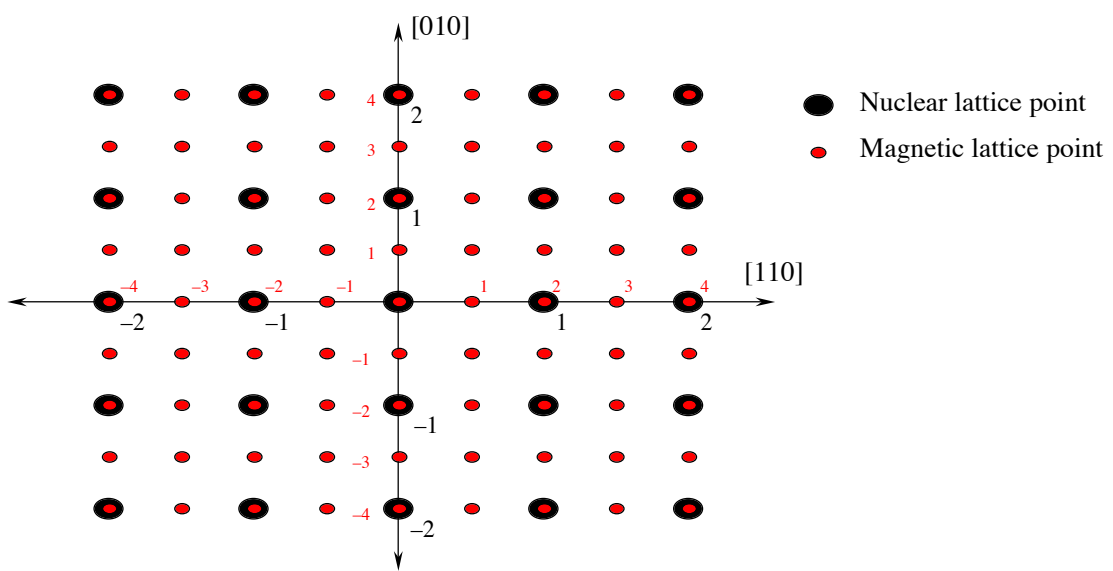


F2.2

The nuclear unit cell is primitive, thus Bragg peaks will appear at all the points in h , k and l .

F2.3

The magnetic unit cell is twice as large as the nuclear in a , b and c , hence the magnetic reciprocal lattice is half the size of the nuclear reciprocal lattice.



Nuclear indices written in black, magnetic in red.

F2.4

The magnetic structure factor is given by the Fourier transform of the moment orientations and positions, i.e.

$$F_{mag}^{hkl} = \sum_{j=1}^N \mu_j \exp\left(2\pi i(hx_j + ky_j + lz_j)\right)$$

where N is the number of moments in the unit cell. There are 8:

Atom	(x,y,z)	Moment amplitude
1	(0, 0, 0)	+1
2	(0.5, 0.5, 0)	+1
3	(0.5, 0, 0.5)	+1
4	(0, 0.5, 0.5)	+1
5	(0.5, 0, 0)	-1
6	(0, 0.5, 0)	-1
7	(0, 0, 0.5)	-1
8	(0.5, 0.5, 0.5)	-1

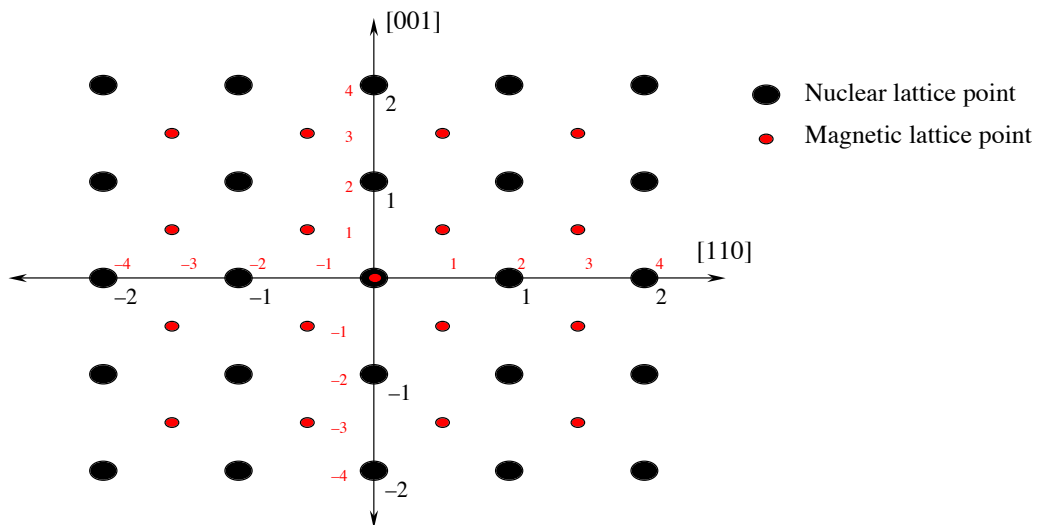
Note that (x,y,z) are defined with respect to the *magnetic* unit cell, and the amplitude is given in units of μ .

Substitute these values in to the equation, which becomes:

$$F_{mag}^{hkl} = \mu \left(1 + \exp(\pi i(h+k)) + \exp(\pi i(h+l)) + \exp(\pi i(k+l)) - \exp(\pi i h) - \exp(\pi i k) - \exp(\pi i l) - \exp(\pi i(h+k+l)) \right)$$

This equals zero for all h,k,l except when they are all odd!

The Bragg peak map therefore looks like:



This comes about because the magnetic unit cell has a higher symmetry than the nuclear unit cell. It is, in fact, face-centred cubic with 4 moments in its basis.

The structure factor for all the visible lattice points is 8μ , however the intensities of the Bragg peaks will *not* be all the same (despite them all having the same structure factor). The direction of \mathbf{Q} with respect to the moment direction becomes important. Neutrons only ever see the perpendicular component of the sublattice magnetization to \mathbf{Q} , thus the intensity of the Bragg peaks will be multiplied by $\sin^2\phi$, where ϕ is the angle between \mathbf{Q} and [001].

Furthermore, the intensity will be modulated by the magnetic form factor. This will cause the intensity to *decrease* with *increasing Q*.

F2.5

The spin waves will be visible in both directions. However, the spin waves in the classical picture take the form of fluctuations that are perpendicular to the mean moment direction. Hence, if the moments are oriented along c , the spin waves will take the form of fluctuations in the (a, b) plane.

Measurements along the [001] axis will therefore see the full contribution from the spin waves as this direction is normal to the (a, b) plane, as \mathbf{Q} is always perpendicular to the moment contributions. Measurements along the [110] axis will only have half this intensity as components of the spin waves along [110] will not give any neutron scattering.

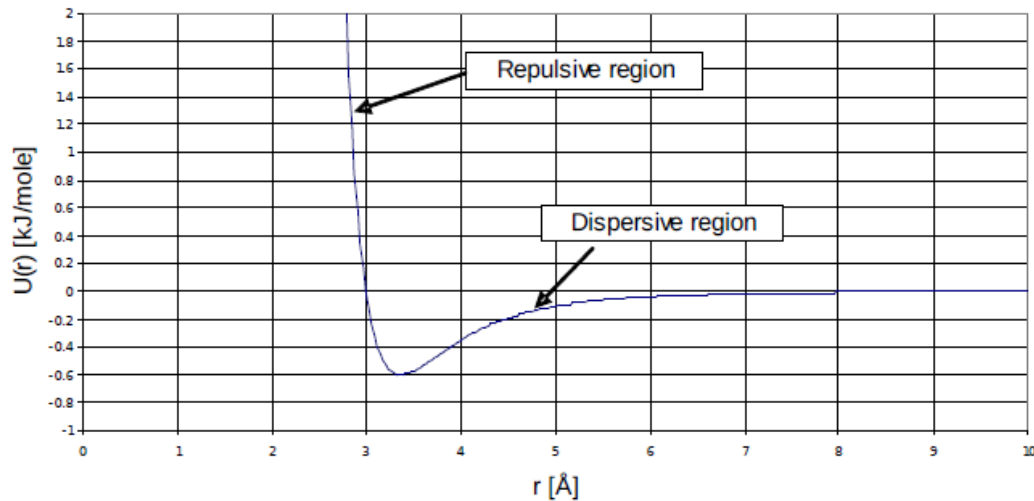
F2.6

If the sample has many domains, there will be no distinction between moments lying along a , b , or c . Therefore the $\sin^2\phi$ term will need to be averaged over all possible orientations, i.e. the magnetic (511) and (333) peaks (which have the same Q) will have the same intensity.

G. Disordered Materials Diffraction

G1.1 a) and c)

Lennard-Jones potential

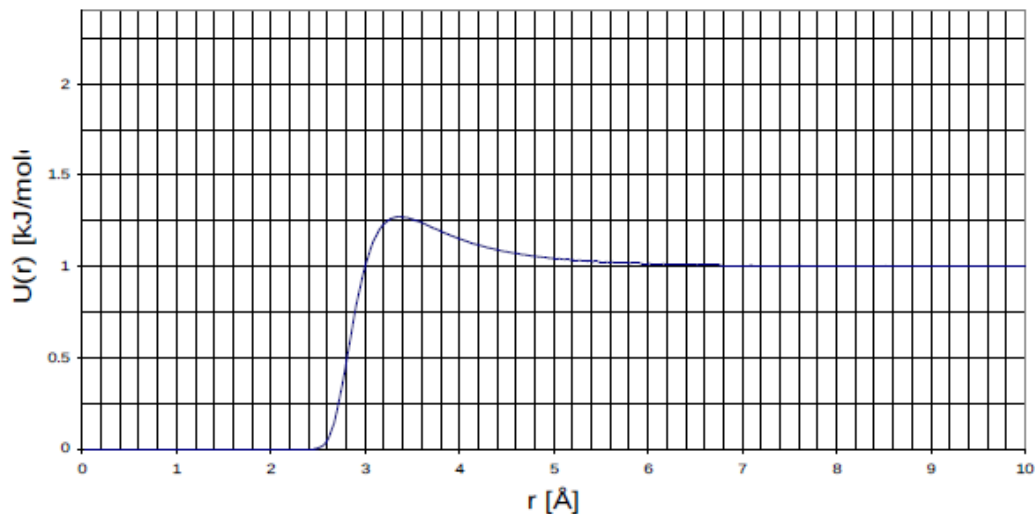


G1.1 b)

ϵ represents the depth of the potential. It controls how tightly adjacent atoms are bound. σ represents the radius at which the hard core repulsive region goes to zero. It represents roughly the distance of closest approach of two atoms.

G1.2 a)

Lennard-Jones gas g(r) at 300K



G1.2b)

At low r , $U(r)$ becomes very large, while $g(r)$ goes to zero. At high r , $U(r)$ goes to zero, while $g(r)$ goes to unity. In between the two functions are in rough antiphase.

G1.2c) If ϵ were increased by a factor of 2, the height of the peak in $g(r)$ at $\sim 3.8\text{\AA}$ would grow from ~ 1.27 to ~ 1.54 . If σ were increased by 20%, the main peak would move out by 20%, but would remain the same height.

G1.3a)

In the gas form $g(r)$ decays monotonically to unity at large r . As the density increases the height of the main peak increases and it becomes sharper as a series of decaying oscillations occur towards larger r . All the peaks move to smaller r with increasing density.

Based on a change of density of 0.02 to 0.035, one might expect the separation of peaks to change by the cube root of the ratio of densities, namely

$$\sqrt[3]{0.02/0.035} = 0.83$$

In fact the first peak moves from 3.18\AA to 3.06\AA , a fractional change of only 0.96, while the second peak moves from 6.39\AA to 5.91\AA , a fractional change of 0.92. In other words the peaks in $g(r)$ do NOT represent the mean separation of the atoms. This can be quite confusing!

G1.3b)

Fundamentally as the material becomes more dense the direct interactions between atoms 1 and 2 become increasingly affected by the presence of 3rd, 4th , etc. atoms which increasingly surround them, and which increasingly confine them in space. Within the pairwise additive approximation assumed here all the atoms interact via known pairwise forces, but the result is many body correlations which are difficult to predict accurately. A raft of theoretical methods to do this approximately exist, but few if any of them work for the kind of interatomic forces that are found in real materials. Hence in practice one has little option but to use computer simulation to determine the effect of many-body correlations in real materials. This problem affects crystals as much as it affects liquids, but in a crystal one has a repeat lattice (which is itself a consequence of many body correlations) which we can determine from the position and height of the Bragg peaks. In any case the primary goal of interest in crystallography is the single particle correlation function (the lattice),

not the higher order correlations. The single particle correlation function for a liquid is uniform and contains no information. For a glass it is not uniform, but contains no repeat distances.

G1.4a)

For density 0.02 the first minimum occurs at 4.95\AA , giving a coordination number of ~ 10 atoms. For density 0.035, the first minimum is at 4.47\AA with a coordination number of 12.5. Clearly these numbers do not scale with density change: coordination number varies less rapidly than the density.

G1.4b)

If instead we had used the same radius, 4.47\AA , then the coordination number at density 0.02 is 7.23, a ratio of 0.58 compared to density 0.035, which is quite close to the ratio of densities, 0.57. This illustrates again that peaks and dips in $g(r)$ do not correlate directly with the density, although they are obviously related to it.

G1.5a)

The primary effect of changing the density on the structure factor is to increase the amplitude of the oscillations. There is some movement of the peaks as well, but fundamentally as the density increases they become sharper, and the oscillations extend to large Q .

G1.5b)

For density 0.02, the first peak in $g(r)$ is at 3.18\AA and the first peak in $S(Q)$ is at 2.2\AA^{-1} . For density 0.035, the first peak in $g(r)$ is at 3.06\AA and the first peak in $S(Q)$ is at 2.35\AA^{-1} , i.e. as the peaks in $g(r)$ move in, those in $S(Q)$ move out, although the movement of the first peak in $S(Q)$ is more related to the movement of the 2nd and subsequent peaks in $g(r)$ than it is to the first peak in $g(r)$.

G1.5c)

It depends how we did it. If we increased σ at constant density, then the peaks would move out, but also become markedly sharper as the packing fraction of the liquid increased. If the density was reduced to compensate for the increase (atoms occupying more space) then the peaks in $S(Q)$ would move in, but without increased amplitude.

G1.5d)

Since the structure factor only exists if the density is finite, a zero density will produce zero structure factor.

G2.1a)

Atomic fractions are $c_{\text{Zn}} = 1/3 = 0.333$, $c_{\text{Cl}} = 2/3 = 0.667$

G2.1b)

$$F(Q) = \frac{1}{9} b_{\text{Zn}}^2 H_{\text{ZnZn}}(Q) + \frac{4}{9} b_{\text{Zn}} b_{\text{Cl}} H_{\text{ZnCl}}(Q) + \frac{4}{9} b_{\text{Cl}}^2 H_{\text{ClCl}}(Q)$$

G2.1c)

In essence the idea is that we measure $F(Q)$ for three samples, namely one with only ^{35}Cl isotope present, another with only ^{37}Cl isotope present, and a third with a mixture of x parts ^{35}Cl and $(1-x)$ parts of ^{37}Cl . For this third sample the chlorine scattering length is

$$b_{\text{mix}} = x b_{^{35}\text{Cl}} + (1-x) b_{^{37}\text{Cl}}$$

which means the weighting coefficient of the H_{ClCl} partial structure factor for this sample is not a linear combination of the same coefficient for the other two samples. This means the determinant of coefficients in the above formula for the three samples is finite and the matrix of coefficients can be inverted. Hence the three measurements can be used to extract the three partial structure factors, at least in principle.

A basic assumption of the isotope substitution method is that the partial structure factors do not change appreciably with isotopic composition of the sample. This is an accurate assumption in most cases, but is less accurate when hydrogen is replaced with deuterium, particularly at low temperatures and with larger molecules, because in these cases quantum effects due to the different masses can impact on both the structure and the phase diagram of the material in question.

G2.1d)

Remarkably few in practice. There have been attempts to perform isomorphic substitution with X-rays, but these method tends to be shrouded in uncertainties from knowing whether one atom can substitute for another without . Then there has been the combination of neutrons, X-rays and electrons, but each technique requires quite different sample containment, making comparisons of the three results dubious. A more promising approach is the use of anomalous dispersion of Xrays, whereby you vary the scattering length of one component near an absorption edge. This method is quite promising, but requires highly stable precision equipment to be performed satisfactorily, and to date has only be tried on a handful of materials. It suffers also from poor counting statistics because of the high degree of monochromatisation needed for the incident beam of X-rays.

Recently we have been exploring the use EXAFS to refine liquid and glass structures, and this approach looks very promising indeed.

G2.2a)

This is a very common problem in neutron scattering using isotopes: one or more of the components makes only a small contribution to the scattering pattern. In this case it is the ZnZn structure factor. Below is shown the inversion of the weights matrix:-

Partial Structure Factor	$\text{Zn}^{35}\text{Cl}_2$	$\text{Zn}^{\text{mix}}\text{Cl}_2$	$\text{Zn}^{37}\text{Cl}_2$
Zn-Zn	37.25	-71.53	62.16
Zn-Cl	-21.87	39.37	-17.50
Cl-Cl	10.15	-14.99	4.84

Table II: Inversion of the matrix coefficients of Table I

You will notice that to extract the ZnZn partial structure factor we need to multiply the data by large numbers and then add and subtract them, making us rely heavily on the absolute accuracy of the diffraction data if we are to avoid amplifying systematic data errors in the final structure factor.

Obtaining absolute scattering cross sections with accuracies better than 1% is a tall order with any technique, including neutrons, and is rarely achieved.

G2.2b)

Particular difficulties are:-

- a) The data are only available over a finite Q range;
- b) The data are multiplied by Q in the integrand of (1.5) making the effect of statistical uncertainty at high Q a particular difficulty.
- c) No matter how careful they are measured and corrected, diffraction data always have systematic errors, which can seriously perturb the Fourier transform, particularly at low r.

Fourier transform of data with potential significant systematic error is risky: the systematic error can have the effect of introducing marked backgrounds in real space that can make the peaks larger or smaller than they should be. As a consequence coordination numbers can be faulty when extracted by this method.

G2.2c)

Fourier transforms of raw data should be avoided whenever possible. Instead the data should be compared with a structural model of the data, and then, assuming the model is satisfactory, use the model to generate the real space distributions, as well as address other questions about the structure of the material. Computer simulation is a convenient method to produce such a structural model of the measured scattering cross sections. This model will also help to identify what might be wrong (if there is anything) with the data, and avoid some of the problems introduced by systematic effects. Some authorities are reluctant to use computer simulation to achieve this, since it too can introduce systematic bias in the interpretation of the data, and so instead invoke a series of consistency checks on the data. These are used to identify and correct particular problems with the data, but this can be a very time consuming process which can take months to resolve. The net effect is the same however: in computer simulation one is already applying a series of physical consistency checks on the data, with the advantage that you have at the end a physical model of the scattering system which is consistent with your scattering data. With the other methods, you have corrected data, but you still have the problem of trying to understand what they mean.

G2.3a)

Figure G2.2 shows the running coordination number of this $g(r)$. From this graph we can read that at the first minimum, 3.4\AA , the running coordination number is ~ 4.3 Cl about Zn. Since there are half the number Zn atoms compared to Cl, the coordination number of Zn about Cl will be 2.2.

G2.3b)

The first ZnCl peak is at 2.31\AA , while the first ClCl distance is at 3.69\AA . Using the cosine rule, I estimate the Cl-Zn-Cl angle to be 106° , which is close to the tetrahedral angle of 109.47° . This together with the coordination number of ~ 4 is a strong hint of likely tetrahedral local coordination in this liquid.

Taking this argument a bit further, one notices that the first ZnZn peak is at 3.93\AA , while the second is at 6.81\AA , giving a Zn-Zn-Zn angle of 120° , suggesting also that at least the Zn packing is not simple, and probably maps into the roughly tetrahedral packing of the Cl around Zn, with significant edge-sharing of the tetrahedra.

G2.3c)

Looking at the curves one is struck by the way the ZnCl oscillations are almost exactly out of phase with the ZnZn and ClCl oscillations. This behaviour strongly indicative of charge ordering, although it is not entirely clear that Zn and Cl are fully ionic in this system.

H: Polarized Neutrons

H1. a) Flipping ratio: $F = N_+ / N_- = 51402 / 1903 = 27 \pm 0.6$

$$\{\text{error bar } dF = \sqrt{\left(\frac{dN_+}{N_-}\right)^2 + \left(\frac{dN_- N_+}{N_-^2}\right)^2} \Rightarrow dF = 0.63\}$$

Therefore, the polarization is: $P = F - 1 / F + 1 = 0.929 \pm 0.002$

$$\{\text{error bar } dP = \left(\frac{2}{(F+1)^2}\right)dF \Rightarrow dF = 0.002\}$$

b) Systematic errors in this measurement will largely arise from background contributions from the instrumental environment. In order to measure a reliable flipping ratio, the N_+ and N_- counts must be measured with and without the sample in the beam. The flipping ratio is then given by

$$F = \frac{N_+^{\text{sample}} - N_+^{\text{empty}}}{N_-^{\text{sample}} - N_-^{\text{empty}}}$$

Other sources of systematic error will be different values of the polarizing power of the polarizer and analyser, in addition to the finite flipping efficiency of the flipper.

H2. a) The adiabacity parameter is given by $E = \frac{\omega_L}{\omega_B}$

The Larmor frequency, $\omega_L = \gamma B$, where the gyromagnetic ratio, γ , is given by the ratio of the neutron magnetic moment to its angular momentum ($= \frac{1}{2}\hbar$). Therefore: $\omega_L = 2\mu_B B / \hbar = 1.83 \times 10^8 B \text{ rad s}^{-1}$ with B given in T.

In this example, $B = 3 \text{ mT}$ and is constant in magnitude, therefore

$$\omega_L = 5.49 \times 10^5 \text{ rad s}^{-1}$$

The rotation frequency of the guide field in the neutron rest frame is

$$\omega_B = \frac{d\theta}{dx} \times v = \frac{\frac{\pi}{2}}{0.1} \times v = 15.71v$$

Expressing v in terms of λ :

$$E = \frac{h^2}{2m_n\lambda^2} = \frac{m_nv^2}{2} \Rightarrow v = \frac{h}{m_n\lambda} = \frac{3956}{\lambda} \text{ with } v \text{ in ms}^{-1} \text{ and } \lambda \text{ in } \text{\AA}.$$

Therefore:

$$\omega_B = 3.11 \times 10^4 \text{ rad s}^{-1}$$

The adiabacity parameter is therefore: **E = 17.7** and the field/flipper design should successfully propagate the neutron polarization and flip the spins without significant depolarization.

b) The design could be improved by either increasing the guide fields (and the current in the Dabbs foil) or by lengthening the distance over which the field rotates by 90°.

H3. a) The number of neutrons transmitted through an absorbing material is:

$$n = n_0 \exp(-N\sigma t)$$

where n_0 is the initial number of neutrons, N is the number density of atoms in the material, σ is the mean absorption cross-section and t is the thickness of the material. So the numbers of + and - neutrons transmitted is:

$$\begin{aligned} n_+ &= n_0 \exp(-N\sigma_+ t) = n_0 \exp(-N\sigma_0 t) \exp(-N\sigma_p t) \\ n_- &= n_0 \exp(-N\sigma_- t) = n_0 \exp(-N\sigma_0 t) \exp(N\sigma_p t) \end{aligned}$$

Therefore the polarization is:

$$P = \frac{n_+ - n_-}{n_+ + n_-} = \frac{\exp(-N\sigma_p t) - \exp(N\sigma_p t)}{\exp(-N\sigma_p t) + \exp(N\sigma_p t)} = -\tanh(N\sigma_p t)$$

The transmission of each spin state is:

$$T_{\pm} = \frac{n_{\pm}}{n_0} = \exp(N\sigma_{\pm} t)$$

Therefore the total transmission is:

$$T = \frac{T_+ + T_-}{2} = \exp(-N\sigma_0 t) \frac{\exp(-N\sigma_p t) + \exp(N\sigma_p t)}{2} = \exp(-N\sigma_0 t) \cosh(N\sigma_p t)$$

b) The expression for the spin-dependent absorption of a ${}^3\text{He}$ spin filter is

$$\sigma_{\pm} = \sigma_0(1 \mp P_{He})$$

where, P_{He} is the nuclear polarization and σ_0 is the energy dependent absorption cross-section.

We now have two expressions for the spin-dependent absorption;

$$\sigma_{\pm} = \sigma_0(1 \mp P_{He}) = \sigma_0 \pm \sigma_p$$

So, equating the spin-dependent parts of the expression, we get

$$\sigma_p = -\sigma_0 P_{He} \Rightarrow P_{He} = -\frac{\sigma_p}{\sigma_0}$$

Substituting this back into the general expressions for the spin-filter polarization and transmission, we get:

$$P = \tanh(P_{He} N \sigma_0 t) \text{ and } T = \exp(-N \sigma_0 t) \cosh(P_{He} N \sigma_0 t)$$

- H4.** a) The expression for the differential cross-section of a polarized neutron beam of polarization (\mathbf{P}) from a ferromagnetic crystal magnetised along the direction ($\mathbf{\eta}$) reflecting from the HKL Bragg plane, is of the form

$$\frac{d\sigma}{d\Omega} = F_N^2 + F_M^2 + 2F_N F_M [\mathbf{P} \cdot \hat{\mathbf{\eta}}]$$

If we consider an initially unpolarized beam as a superposition of equal populations of “spin-up” and “spin-down” neutrons, then the number of neutrons scattered in each spin-state will be proportional to the two cross sections.

$$\begin{aligned} n_+ &\propto \left. \frac{d\sigma}{d\Omega} \right|_{\mathbf{P} \parallel \mathbf{\eta}} = (F_N + F_M)^2 \\ n_- &\propto \left. \frac{d\sigma}{d\Omega} \right|_{\mathbf{P} \perp \mathbf{\eta}} = (F_N - F_M)^2 \end{aligned}$$

Therefore, the polarization is:

$$P = \frac{n_+ - n_-}{n_+ + n_-} = \frac{(F_N + F_M)^2 - (F_N - F_M)^2}{(F_N + F_M)^2 + (F_N - F_M)^2} = \frac{2F_N F_M}{F_N^2 + F_M^2}$$

Note that the sign of the polarization depends on the signs of the unsquared magnetic and nuclear structure factors. In the case of Heusler alloy, these signs are opposite, and the polarization is oriented opposite to the magnetisation (i.e. spin-down)

b) Making the substitution, $x = F_N/F_M$, we have

$$P = \frac{2x}{x^2+1}$$

Differentiating with respect to x

$$\frac{dP}{dx} = \frac{2-2x^2}{(x^2+1)^2}$$

The maximum polarization is therefore found for $x = \pm 1$. i.e. When the nuclear and magnetic structure factors are equal.

H5. The first rule of thumb in magnetic polarized neutron scattering is that spin-flipped neutrons will only be produced by components of the sample magnetisation perpendicular to the neutron polarization direction. [This is an extremely useful rule to bear in mind during all polarized neutron experiments.] Therefore, if we are scattering neutrons from a fully magnetised scatterer (i.e. a ferromagnet for example) – magnetised in the direction of the neutron polarization (which is an experiment necessity), then there will be no perpendicular components of the magnetisation, and therefore no spin-flip scattering. We can therefore dispense with the analysers, since the scattered beam remains fully polarized

H6. a) The Pauli spin relations are:

$$\sigma_x |\uparrow\rangle = \begin{bmatrix} 0 & 1 \\ 1 & 0 \end{bmatrix} \begin{bmatrix} 1 \\ 0 \end{bmatrix} = \begin{bmatrix} 0 \\ 1 \end{bmatrix} = |\downarrow\rangle$$

$$\sigma_x |\downarrow\rangle = \begin{bmatrix} 0 & 1 \\ 1 & 0 \end{bmatrix} \begin{bmatrix} 0 \\ 1 \end{bmatrix} = \begin{bmatrix} 1 \\ 0 \end{bmatrix} = |\uparrow\rangle$$

$$\sigma_y |\uparrow\rangle = \begin{bmatrix} 0 & -i \\ i & 0 \end{bmatrix} \begin{bmatrix} 1 \\ 0 \end{bmatrix} = i \begin{bmatrix} 0 \\ 1 \end{bmatrix} = i |\downarrow\rangle$$

$$\sigma_x |\downarrow\rangle = \begin{bmatrix} 0 & -i \\ i & 0 \end{bmatrix} \begin{bmatrix} 0 \\ 1 \end{bmatrix} = -i \begin{bmatrix} 1 \\ 0 \end{bmatrix} = -i |\uparrow\rangle$$

$$\sigma_z |\uparrow\rangle = \begin{bmatrix} 1 & 0 \\ 0 & -1 \end{bmatrix} \begin{bmatrix} 1 \\ 0 \end{bmatrix} = \begin{bmatrix} 1 \\ 0 \end{bmatrix} = |\uparrow\rangle$$

$$\sigma_z |\downarrow\rangle = \begin{bmatrix} 1 & 0 \\ 0 & -1 \end{bmatrix} \begin{bmatrix} 0 \\ 1 \end{bmatrix} = - \begin{bmatrix} 0 \\ 1 \end{bmatrix} = - |\downarrow\rangle$$

b) Now, we have to calculate the matrix element for magnetic scattering $\langle S' | V_m | S \rangle$, where S' and S are the final and initial spin states, and V_m is the magnetic interaction potential, which is given by

$$V_m = \frac{-\gamma_n r_0}{2m_n} \sum_{\xi} \sigma_{\xi} M_{\perp\xi}$$

Therefore, the 4 possible spin-transitions are given by

i) Non-spin-flip: $|\uparrow\rangle \rightarrow |\uparrow\rangle$

$$\begin{aligned}\langle \uparrow | V_m | \uparrow \rangle &= \frac{-\gamma_n r_0}{2m_n} (\langle \uparrow | \sigma_x | \uparrow \rangle M_{\perp x} + \langle \uparrow | \sigma_y | \uparrow \rangle M_{\perp y} + \langle \uparrow | \sigma_z | \uparrow \rangle M_{\perp z}) \\ &= \frac{-\gamma_n r_0}{2m_n} (\langle \uparrow | \downarrow \rangle M_{\perp x} + i \langle \uparrow | \downarrow \rangle M_{\perp y} + \langle \uparrow | \uparrow \rangle M_{\perp z}) \\ &= \frac{-\gamma_n r_0}{2m_n} M_{\perp z}\end{aligned}$$

ii) Non-spin-flip: $|\downarrow\rangle \rightarrow |\downarrow\rangle$

$$\begin{aligned}\langle \downarrow | V_m | \downarrow \rangle &= \frac{-\gamma_n r_0}{2m_n} (\langle \downarrow | \sigma_x | \downarrow \rangle M_{\perp x} + \langle \downarrow | \sigma_y | \downarrow \rangle M_{\perp y} + \langle \downarrow | \sigma_z | \downarrow \rangle M_{\perp z}) \\ &= \frac{-\gamma_n r_0}{2m_n} (\langle \downarrow | \uparrow \rangle M_{\perp x} - i \langle \downarrow | \uparrow \rangle M_{\perp y} - \langle \downarrow | \downarrow \rangle M_{\perp z}) \\ &= \frac{-\gamma_n r_0}{2m_n} (-M_{\perp z})\end{aligned}$$

iii) Spin-flip: $|\uparrow\rangle \rightarrow |\downarrow\rangle$

$$\begin{aligned}\langle \downarrow | V_m | \uparrow \rangle &= \frac{-\gamma_n r_0}{2m_n} (\langle \downarrow | \sigma_x | \uparrow \rangle M_{\perp x} + \langle \downarrow | \sigma_y | \uparrow \rangle M_{\perp y} + \langle \downarrow | \sigma_z | \uparrow \rangle M_{\perp z}) \\ &= \frac{-\gamma_n r_0}{2m_n} (\langle \downarrow | \downarrow \rangle M_{\perp x} + i \langle \downarrow | \downarrow \rangle M_{\perp y} + \langle \downarrow | \uparrow \rangle M_{\perp z}) \\ &= \frac{-\gamma_n r_0}{2m_n} (M_{\perp x} + i M_{\perp y})\end{aligned}$$

iv) Spin-flip: $|\downarrow\rangle \rightarrow |\uparrow\rangle$

$$\begin{aligned}\langle \uparrow | V_m | \downarrow \rangle &= \frac{-\gamma_n r_0}{2m_n} (\langle \uparrow | \sigma_x | \downarrow \rangle M_{\perp x} + \langle \uparrow | \sigma_y | \downarrow \rangle M_{\perp y} + \langle \uparrow | \sigma_z | \downarrow \rangle M_{\perp z}) \\ &= \frac{-\gamma_n r_0}{2m_n} (\langle \uparrow | \uparrow \rangle M_{\perp x} - i \langle \uparrow | \uparrow \rangle M_{\perp y} - \langle \uparrow | \downarrow \rangle M_{\perp z}) \\ &= \frac{-\gamma_n r_0}{2m_n} (M_{\perp x} - i M_{\perp y})\end{aligned}$$

These equations show that the magnetic non-spin-flip scattering is entirely due to the component of the magnetisation parallel to the neutron polarization direction, $M_{\perp z}$; and that the magnetic spin-flip scattering is entirely due to the components of the magnetisation perpendicular to the neutron polarization direction, $M_{\perp x}$ and $M_{\perp y}$.

- H7.** From the previous question (which is a derivation of the magnetic part of the Moon, Riste and Koehler equations) we have established that spin-flip scattering arises solely from the components of the sample magnetisation perpendicular to the neutron polarization.

Now, the definition of the neutron sensitive sample magnetisation in reciprocal space (the “magnetic interaction vector”) is

$$\mathbf{M}_\perp(Q) = \boldsymbol{\eta} - (\boldsymbol{\eta} \cdot \hat{\mathbf{Q}})\hat{\mathbf{Q}}$$

where $\boldsymbol{\eta}$ is the sample magnetisation (see, for example, Squires, or previous lectures on magnetic scattering).

From this equation, we note that if the scattering vector is parallel to the sample magnetisation, then the neutron sensitive magnetisation is zero. Therefore, if the neutron polarization is parallel to the scattering vector, the only components of the magnetisation that will scatter neutrons will be perpendicular to the polarization, and will therefore flip the neutron spins.

- H8.** The advantage of the X-Y-Z difference method of magnetic scattering separation over the method of measuring with the neutron polarization $\mathbf{P} \parallel \mathbf{Q}$, is that the X-Y-Z method applies to a general multi-detector instrument. The $\mathbf{P} \parallel \mathbf{Q}$ method only works for one scattering vector at a time.

A further advantage of X-Y-Z is that it is insensitive to background, since the spin-flip background will be the same in Z, X and Y directions, and will therefore cancel out.

I. High resolution spectroscopy (TOF, backscattering and Spin-Echo)

The aim of this section is to get a feeling for the energy resolution of different spectrometer types: time-of-flight (TOF), backscattering (BS) and spin echo (NSE) spectrometers.

All the following calculations assume a **neutron wavelength of $\lambda=6.3 \text{ \AA}$** .

Planck's constant is $h=6.6225 \cdot 10^{-34} \text{ Js}$, sometimes usefully expressed as $h = 4.136 \text{ \mu eV ns}$. Neutron mass $m_n=1.675 \cdot 10^{-27} \text{ kg}$.

I1.

Calculate the neutron speed v_n in [m/s] and the neutron energy in μeV .
 $v_n = \underline{\hspace{2cm}} 630 \text{ m/s}$; $E_n = \underline{\hspace{2cm}} 2080 \text{ \mu eV}$.

I2. - Time-of-flight spectroscopy

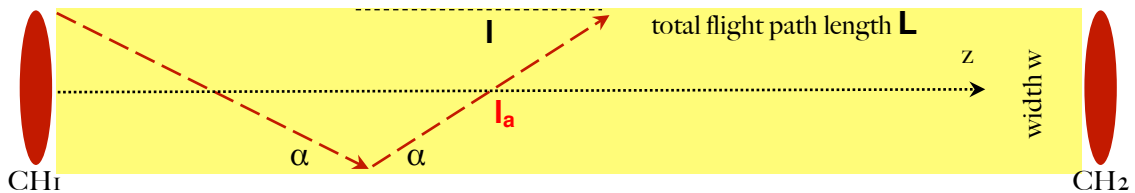


Figure I1. Time-of-flight spectrometer with two choppers CH_1 and CH_2 separated by a distance L

All contributions to the energy resolution in time-of-flight can be formulated as time uncertainty $\Delta t/t$. We consider only the primary spectrometer (before sample) and aim for an energy resolution better than $1 \mu\text{eV}$.

a) Show first that $\Delta E/E = 2\Delta t/t$ (express E as fct. of v and assume $\Delta d = 0$):

$$E = \underline{\hspace{4cm}} \frac{1}{2} mv^2 = \frac{1}{2} m d^2/t^2 \quad \text{and with } \Delta d = 0:$$

$$\Delta E = \underline{\hspace{4cm}} -md^2/t^3 \Delta t, \quad \text{which results in } \Delta E/E = \underline{\hspace{4cm}} 2 \Delta t/t.$$

Several contributions add to the neutron flight time uncertainty Δt . To simplify, let's consider a chopper spectrometer with flight path L between two choppers as sketched in the Figure. I1. and let's first look at neutrons flying parallel to z .

b) Calculate the flight time along path $L = 100 \text{ m}$: $T_0 \sim \underline{\text{0.159}}$ s.
If we want to get an energy resolution of $1 \mu\text{eV}$, this corresponds to
 $\Delta E/E \sim \underline{\text{4.8} \times 10^{-4}}$ for 6.3 \AA neutrons.

This can give us an idea for the maximum allowed flight time difference along L : $\Delta E/E_0 * T_0/2 \sim \underline{\text{38}}$ μsec

c) Path difference in neutron guide

For the reflected neutrons estimate the max. flight path differences in a super-mirror guide with $m=2$ coating and width w . The critical angle α (maximal reflection angle = half divergence) in such a guide is $\alpha \sim 0.1^\circ$ $m \lambda = \underline{\text{1.26}}$ $^\circ$.

Estimate the flight path difference with respect to neutrons which fly parallel. One way is to show that $\Delta L/L = (1/\cos \alpha) - 1$ and thus:

$$\Delta L/L = \underline{\text{2.4} \times 10^{-4}} = \Delta t/t \text{ and therefore:}$$

$$\Delta E/E \sim \underline{\text{4.8} \times 10^{-4}}.$$

We prove this by referring to Figure I1:

$$l = \underline{w/\tan \alpha};$$

$$l_a = \underline{w/\cos \alpha};$$

$l_a/l = \underline{1/\cos \alpha}$ independent of w ; if n is the number of reflections, then we can write the full path difference as:

$$\Delta L = n*(l_a - l) = \underline{(L/l)*(l_a - l) = L(1/\cos \alpha - 1)}$$

and thus $\Delta L/L = (1/\cos \alpha) - 1$.

d) Chopper Opening Time

Another contribution is the chopper opening time which leads to a spread in neutron velocity and thus to flight time differences Δt . In order to reach similar $\Delta t/t = \Delta v/v$ as above one needs fast rotating choppers delivering short pulses.

If CH1 releases at $t = 0$ an arbitrarily sharp pulse of a white beam, then the CH2 delay T selects a neutron velocity v_0 and the CH2 opening time determines $\Delta v/v$.

We want again $1\mu\text{eV}$ energy resolution therefore we need

$$\Delta v/v_0 = \Delta t/T = \underline{\underline{2.4 \times 10^{-4}}}.$$

The chopper opening time must then be

$$\Delta t_{\text{CH2}} < 1/2 * (1\mu\text{eV}/E_0)^*/v_0 = \underline{\underline{3.8 \times 10^{-7}}} [\text{s}/\text{m}] * L [\text{s}].$$

Mechanically, the chopper opening time is defined as: $\Delta t_{\text{CH2}} = \beta / 360 / f$, where β is the chopper window angular opening and $\beta/360$ is the duty cycle (which equals the fraction of neutrons transmitted by the chopper). We see that this condition can be achieved by increasing the flight path (or by decreasing v_n), by increasing the chopper frequency or by narrowing the chopper window (intensity loss).

Choosing a duty cycle of 0.01 one needs a very long flight path between CH1 and CH2 of $L=100\text{m}$ and a high chopper frequency of

$$\underline{\underline{263}} \text{ Hz} = \underline{\underline{15790}} \text{ rpm}$$

to reach $1\mu\text{eV}$ energy resolution.

This condition becomes more restrictive if we consider the finite opening time of the first chopper as well. Finally, we mention that all the contributions in the primary and secondary spectrometer have to be added in quadrature:

$$\Delta t/t = \sqrt{[(\Delta t_1/t_1)^2 + (\Delta t_2/t_2)^2 + \dots]}$$

Additional choppers are usually needed to avoid frame overlap and harmonics, which reduces the intensity further. To achieve a $1\mu\text{eV}$ energy resolution by TOF is technically demanding (choppers), expensive (guides) and low in flux. Thus TOF-chopper-instruments have typically energy resolutions $> 10 \mu\text{eV}$. ex.: IN5 at 6.3\AA has roughly $40 \mu\text{eV}$ energy resolution.

Increasing λ helps but reduces the maximum Q . Calculate the elastic Q for 3\AA , 6\AA and 15\AA neutrons, assuming a maximum scattering angle of 140° :

$$Q = \underline{\underline{4\pi \sin\theta / \lambda}} = \underline{\underline{3.94}} \text{ \AA}^{-1}, \underline{\underline{1.97}} \text{ \AA}^{-1} \text{ and } \underline{\underline{0.98}} \text{ \AA}^{-1}$$

I2. - Backscattering spectroscopy

Reactor backscattering spectrometers are based on perfect crystal optics. High energy resolution is achieved by choosing Bragg angles Θ as close as possible to 90° . Two major terms determine then the energy resolution: the spread in lattice spacing $\Delta d/d$ of the monochromator and the angular deviation ϵ from backscattering direction (the latter includes the beam divergence α if considered as $\epsilon = \alpha/2$).

Write down the Bragg equation (neglecting higher orders):

$$\lambda = 2d \sin\theta \quad \text{or equivalently using } k=2\pi/\lambda \text{ and } \tau = 2\pi/d$$

(reciprocal lattice vector of the Bragg reflection): $k = \tau / (2 \sin\theta)$.

Deduce the wavelength resolution $\Delta\lambda/\lambda$ by differentiating the Bragg equation:

$$\Delta\lambda = \frac{2 \sin\theta \cdot \Delta d}{\lambda} + \frac{2d \cos\theta \cdot \Delta\theta}{\lambda^2} \quad \text{and thus}$$

$$\Delta\lambda/\lambda = \frac{\Delta d}{d} + \frac{\cot\theta \cdot \Delta\theta}{\lambda}, \quad \text{or equivalently:}$$

$$\Delta k = \frac{\Delta\tau}{\lambda} + \frac{\{\tau / (2 \sin^2 \theta)\} \cos\theta \cdot \Delta\theta}{\lambda^2} \quad \text{and thus}$$

$$\Delta k/k = \frac{\Delta\tau}{\tau} + \frac{\cot\theta \cdot \Delta\theta}{\lambda}.$$

The energy resolution is given by two terms. The first one, $\Delta d/d = \Delta\tau/\tau$, can be calculated by dynamical scattering theory as $\Delta\tau/\tau = h^2/m 4 F_\tau N_c$, where F_τ is the structure factor of the reflection used and N_c the number density of atoms in the unit cell. The second one, the angular deviation, can for $\theta \approx 90^\circ$ be expanded in powers of θ and contributes approximately as $\Delta\lambda/\lambda \sim \Delta\theta^2/4$ ($\Delta\theta$ in radians).

Calculate now the contribution to the energy resolution of both terms for a perfect crystal Si(111) monochromator (6.271 Å, but approximate by 6.3 Å as above).

With $F_{\tau=(111)}$ and N_c for Si(111) the extinction contribution for Si(111) in backscattering is $\Delta d/d = 1.86 \cdot 10^{-5}$ and thus $\Delta E/E = 3.46 \times 10^{-5}$ and $\Delta E = 0.07 \mu\text{eV}$.

Estimate the energy resolution contribution due to deviation from backscattering:

1) given by a sample diameter of 4 cm in 2 m distance from the analyser.

$$\Delta E/E = 5 \times 10^{-5}, \Delta E = 0.1 \mu\text{eV}$$

2) given by this sample at 1m distance:

$$\Delta E/E = \underline{2 \times 10^{-5}}, \Delta E = \underline{0.42} \text{ } \mu\text{eV}$$

3) given by a detector being placed near backscattering, a sample - analyser distance of 1m and the distance sample center - detector center = 10cm below the scattering plane; the focus of the analyser sphere is placed in the middle between sample and detector:

$$\Delta E/E = \underline{1.25 \times 10^{-3}}. \Delta E = \underline{2.6} \text{ } \mu\text{eV}$$

These examples show that for small enough deviations from BS energy resolutions of $< 1 \mu\text{eV}$ are easily achievable. Comparing this to TOF contributions above, it becomes clear that for a spallation source backscattering instrument, which combines TOF in the primary spectrometer with near-BS in the secondary spectrometer, it is very difficult to achieve sub- μeV resolution. The SNS BS (BASIS) instrument with 80m flight path has for example an energy resolution for Si(111) of 2.5 μeV .

I3. - Neutron spin-echo spectroscopy

In neutron spin echo one uses the neutron spin which undergoes precessions in a magnetic field B . The precession angle ϕ after a path length L depends on the field integral, given by $\phi = \gamma * B * L / v_n$ (γ = gyromagnetic ratio of the neutron, v_n =neutron speed). For a polychromatic beam the precession angles of the neutron spins will be very different depending on the neutron speed and thus a previously polarized beam becomes depolarized. The trick is then to send the neutrons after the sample through a field with opposite sign and with the same field integral. Therefore, for elastic scattering, the precessions are “turned backwards”, again depending on the neutron velocity, and the full polarization is recovered. This allows the use of a wide wavelength band (range of incident neutron speeds) and therefore a high intensity which is ‘decoupled’ from the energy resolution.

In order to estimate a typically achievable energy resolution, we can calculate the longest time which is easily accessible in NSE.

The NSE time is given by: $t_{NSE} = \hbar \gamma B L / (m_n v_n^3)$ thus it is proportional to the largest achievable field integral $B * L$, which we take as 0.25 [T*m].

Calculate the longest NSE time t_{NSE} for $\lambda=6.3\text{\AA}$ neutrons (use v_n calculated above), knowing that $\gamma = 1.832 \cdot 10^8 [\text{T}^{-1} \text{s}^{-1}]$, $\hbar = 1.054 \cdot 10^{-34} \text{ J s}$; and $m_n = 1.675 \cdot 10^{-27} \text{ kg}$:

$$t_{NSE} = \underline{11.7} \text{ ns.}$$

Convert this time into an energy by multiplying its reciprocal value with $h=4.136 \text{ } \mu\text{eV ns}$; we get: $E_{\text{NSE}} = \underline{\text{0.35}} \text{ } \mu\text{eV}$.

For comparing measurements in time and in energy one often refers to Fourier-transformation which relates e.g. the characteristic relaxation time τ of an exponential relaxation in time to the width of a Lorentzian function in energy by $\tau = 1/\omega$. In spite of the fact that the relaxation time is usually smaller than the longest NSE time, converting the corresponding energy resolution by this relation gives:

$$E_\tau = \underline{\text{0.056}} \text{ } \mu\text{eV}.$$

Because of $\tau < t_{\text{NSE}}$ and also because energy spectrometers can usually resolve better than the HWHM, the comparable resolution energy lies somewhere in between the two values calculated.

Note that the longest NSE time depends on wavelength λ as $t_{\text{NSE}} \propto \underline{\lambda^3}$. Thus the resolution improves fast for increasing λ , but like calculated for the other spectrometers above, the maximum Q is reduced.

